

1 **MitoChime: A Machine-Learning Pipeline for**
2 **Detecting PCR-Induced Chimeras in**
3 **Mitochondrial Illumina Reads**

4 A Special Project Proposal
5 Presented to
6 the Faculty of the Division of Physical Sciences and Mathematics
7 College of Arts and Sciences
8 University of the Philippines Visayas
9 Miag-ao, Iloilo

10 In Partial Fulfillment
11 of the Requirements for the Degree of
12 Bachelor of Science in Computer Science

13 by

14 Duranne Duran
15 Yvonne Lin
16 Daniella Pailden

17 Adviser
18 Francis D. Dimzon, Ph.D.

19 December 5, 2025

Contents

21	1 Introduction	1
22	1.1 Overview	1
23	1.2 Problem Statement	3
24	1.3 Research Objectives	4
25	1.3.1 General Objective	4
26	1.3.2 Specific Objectives	4
27	1.4 Scope and Limitations of the Research	5
28	1.5 Significance of the Research	6
29	2 Review of Related Literature	7
30	2.1 The Mitochondrial Genome	7
31	2.1.1 Mitochondrial Genome Assembly	8

32	2.2 PCR Amplification and Chimera Formation	9
33	2.3 Existing Traditional Approaches for Chimera Detection	10
34	2.3.1 UCHIME	11
35	2.3.2 UCHIME2	12
36	2.3.3 CATch	13
37	2.3.4 ChimPipe	14
38	2.4 Machine Learning Approaches for Chimera and Sequence Quality	
39	Detection	15
40	2.4.1 Feature-Based Representations of Genomic Sequences . . .	15
41	2.5 Synthesis of Chimera Detection Approaches	16
42	3 Research Methodology	19
43	3.1 Research Activities	19
44	3.1.1 Data Collection	20
45	3.1.2 Feature Extraction Pipeline	24
46	3.1.3 Machine Learning Model Development	27
47	3.1.4 Model Benchmarking, Hyperparameter Optimization, and	
48	Evaluation	28
49	3.1.5 Feature Importance and Interpretation	29

50	3.1.6 Validation and Testing	30
51	3.1.7 Documentation	31
52	3.2 Calendar of Activities	32
53	4 Results and Discussion	33
54	4.1 Descriptive Analysis of Features	33
55	4.1.1 Exploratory Data Analysis	34
56	4.2 Baseline Classification Performance	35
57	4.3 Effect of Hyperparameter Tuning	37
58	4.4 Detailed Evaluation of Representative Models	38
59	4.4.1 Confusion Matrices and Error Patterns	39
60	4.4.2 ROC and Precision–Recall Curves	40
61	4.5 Feature Importance and Biological Interpretation	42
62	4.5.1 Permutation Importance of Individual Features	42
63	4.5.2 Feature Family Importance	43
64	4.6 Summary of Findings	45
65	A Histograms of Key Features	47

⁶⁶ List of Figures

⁶⁷	3.1 Process Diagram of Special Project	20
⁶⁸	4.1 Feature correlation heatmap showing relationships among alignment-	
⁶⁹	derived and sequence-derived variables.	35
⁷⁰	4.2 Test F1 of all baseline classifiers, showing that no single model	
⁷¹	clearly dominates and several achieve comparable performance. . .	36
⁷²	4.3 Comparison of test F1 (left) and ROC–AUC (right) for baseline and	
⁷³	tuned models. Hyperparameter tuning yields small but consistent	
⁷⁴	gains, particularly for tree-based ensembles.	38
⁷⁵	4.4 Confusion matrices for the four representative models on the held-	
⁷⁶	out test set. All models show more false negatives (chimeric reads	
⁷⁷	called clean) than false positives.	40
⁷⁸	4.5 ROC (left) and precision–recall (right) curves for the four represen-	
⁷⁹	tative models on the held-out test set. Tree-based ensembles cluster	
⁸⁰	closely, with logistic regression performing slightly but consistently	
⁸¹	worse.	41

82	4.6 Permutation-based feature importance for four representative clas-	
83	sifiers. Clipping and k-mer composition features are generally the	
84	strongest predictors, whereas microhomology and other alignment	
85	metrics contribute minimally.	43
86	4.7 Aggregated feature family importance across four models. Clipping	
87	and k-mer compositional shifts are consistently the dominant con-	
88	tributors, while SA_structure, Micro_homology, and other features	
89	contribute minimally.	45
90	A.1 Histogram plots of six key features comparing clean and chimeric	
91	reads.	48

92 List of Tables

⁹⁷ **Chapter 1**

⁹⁸ **Introduction**

⁹⁹ **1.1 Overview**

¹⁰⁰ The rapid advancement of next-generation sequencing (NGS) technologies has
¹⁰¹ transformed genomic research by enabling high-throughput and cost-effective
¹⁰² DNA analysis (Metzker, 2010). Among current platforms, Illumina sequencing
¹⁰³ remains the most widely adopted, capable of producing millions of short reads
¹⁰⁴ that can be assembled into reference genomes or analyzed for genetic variation
¹⁰⁵ (Bentley et al., 2008; Glenn, 2011). Despite its high base-calling accuracy,
¹⁰⁶ Illumina sequencing is prone to artifacts introduced during library preparation,
¹⁰⁷ particularly polymerase chain reaction (PCR)-induced chimeras, which are ar-
¹⁰⁸ tificial hybrid sequences that do not exist in the true genome (Judo, Wedel, &
¹⁰⁹ Wilson, 1998).

¹¹⁰ PCR chimeras form when incomplete extension products from one template

anneal to an unrelated DNA fragment and are extended, creating recombinant reads (Qiu et al., 2001). In mitochondrial genome assembly, such artifacts are especially problematic because the mitochondrial genome is small, circular, and often repetitive (Boore, 1999; Cameron, 2014). Even a small number of chimeric or misjoined reads can reduce assembly contiguity and introduce false junctions during organelle genome reconstruction (Dierckxsens, Mardulyn, & Smits, 2017; Hahn, Bachmann, & Chevreux, 2013; Jin et al., 2020). Existing assembly tools such as GetOrganelle and MITObim assume that input reads are largely free of such artifacts (Hahn et al., 2013; Jin et al., 2020). Consequently, undetected chimeras may produce fragmented assemblies or misidentified organellar boundaries. To ensure accurate reconstruction of mitochondrial genomes, a reliable method for detecting and filtering PCR-induced chimeras before assembly is essential.

This study focuses on mitochondrial sequencing data from the genus *Sardinella*, a group of small pelagic fishes widely distributed in Philippine waters. Among them, *Sardinella lemuru* (Bali sardinella) is one of the country's most abundant and economically important species, providing protein and livelihood to coastal communities (Labrador, Agmata, Palermo, Ravago-Gotanco, & Pante, 2021; Willette, Bognot, Mutia, & Santos, 2011). Accurate mitochondrial assemblies are critical for understanding its population genetics, stock structure, and evolutionary history. However, assembly pipelines often encounter errors or fail to complete due to undetected chimeric reads. To address this gap, this research introduces MitoChime, a machine learning pipeline designed to detect and filter PCR-induced chimeric reads using both alignment-based and sequence-derived statistical features. The tool aims to provide bioinformatics laboratories, partic-

₁₃₆ ularly the Philippine Genome Center Visayas (PGC Visayas), with an efficient
₁₃₇ solution for improving mitochondrial genome reconstruction.

₁₃₈ 1.2 Problem Statement

₁₃₉ While NGS technologies have revolutionized genomic data acquisition, the ac-
₁₄₀ curacy of mitochondrial genome assembly remains limited by artifacts produced
₁₄₁ during PCR amplification. These chimeric reads can distort assembly graphs and
₁₄₂ cause misassemblies, with particularly severe effects in small, circular mitochon-
₁₄₃ drial genomes (Boore, 1999; Cameron, 2014). Existing assembly pipelines such
₁₄₄ as GetOrganelle, MITObim, and NOVOPlasty assume that sequencing reads are
₁₄₅ free of such artifacts (Dierckxsens et al., 2017; Hahn et al., 2013; Jin et al., 2020).
₁₄₆ At PGC Visayas, several mitochondrial assemblies have failed or yielded incom-
₁₄₇ plete contigs despite sufficient coverage, suggesting that undetected chimeric reads
₁₄₈ compromise assembly reliability. Meanwhile, existing chimera detection tools such
₁₄₉ as UCHIME and VSEARCH were developed primarily for amplicon-based com-
₁₅₀ munity analysis and rely heavily on reference or taxonomic comparisons (Edgar,
₁₅₁ Haas, Clemente, Quince, & Knight, 2011; Rognes, Flouri, Nichols, Quince, &
₁₅₂ Mahé, 2016). These approaches are unsuitable for single-species organellar data,
₁₅₃ where complete reference genomes are often unavailable. Therefore, there is a
₁₅₄ pressing need for a reference-independent, data-driven tool capable of detecting
₁₅₅ and filtering PCR-induced chimeras in mitochondrial sequencing datasets.

₁₅₆ **1.3 Research Objectives**

₁₅₇ **1.3.1 General Objective**

₁₅₈ This study aims to develop and evaluate a machine learning-based pipeline (Mi-
₁₅₉ toChime) that detects PCR-induced chimeric reads in *Sardinella lemuru* mito-
₁₆₀ chondrial sequencing data in order to improve the quality and reliability of down-
₁₆₁ stream mitochondrial genome assemblies.

₁₆₂ **1.3.2 Specific Objectives**

₁₆₃ Specifically, the study aims to:

- ₁₆₄ 1. construct simulated *Sardinella lemuru* Illumina paired-end datasets contain-
₁₆₅ ing both clean and PCR-induced chimeric reads,
- ₁₆₆ 2. extract alignment-based and sequence-based features such as k-mer compo-
₁₆₇ sition, junction complexity, and split-alignment counts from both clean and
₁₆₈ chimeric reads,
- ₁₆₉ 3. train, validate, and compare supervised machine-learning models for classi-
₁₇₀ fying reads as clean or chimeric,
- ₁₇₁ 4. determine feature importance and identify indicators of PCR-induced
₁₇₂ chimerism,
- ₁₇₃ 5. integrate the optimized classifier into a modular and interpretable pipeline
₁₇₄ deployable on standard computing environments at PGC Visayas.

175 1.4 Scope and Limitations of the Research

176 This study focuses on detecting PCR-induced chimeric reads in Illumina paired-
177 end mitochondrial sequencing data from *Sardinella lemuru*. The decision to re-
178 strict the taxonomic scope to a single species is based on four considerations: to
179 limit interspecific variation in mitochondrial genome size, GC content, and repeti-
180 tive regions so that differences in read patterns can be attributed more directly to
181 PCR-induced chimerism; to align the analysis with relevant *S. lemuru* sequencing
182 projects at PGC Visayas; to take advantage of the availability of *S. lemuru* mito-
183 chondrial assemblies and raw datasets in public repositories such as the National
184 Center for Biotechnology Information (NCBI), which facilitates reference selection
185 and benchmarking; and to develop a tool that directly supports local studies on
186 *S. lemuru* population structure and fisheries management.

187 The study emphasizes `wgsim`-based simulations and selected empirical mito-
188 chondrial datasets from *S. lemuru*. It excludes naturally occurring chimeras, nu-
189 clear mitochondrial pseudogenes (NUMTs), and large-scale assembly rearrange-
190 ments in nuclear genomes. Feature extraction is restricted to low-dimensional
191 alignment and sequence statistics, such as k-mer frequency profiles, GC content,
192 read length, soft and hard clipping metrics, split-alignment counts, and map-
193 ping quality, rather than high-dimensional deep learning embeddings. This de-
194 sign keeps model behaviour interpretable and ensures that the pipeline can be
195 run on standard workstations at PGC Visayas. Testing on long-read platforms
196 (e.g., Nanopore, PacBio) and other taxa is outside the scope of this project; the
197 implemented pipeline is evaluated only on short-read *S. lemuru* datasets.

198 Other limitations in this study include the following: simulations with varying

199 error rates were not performed, so the effect of different sequencing errors on model
200 performance remains unexplored; alternative parameter settings, including k-mer
201 lengths and microhomology window sizes, were not systematically tested, which
202 could affect the sensitivity of both k-mer and microhomology feature detection as
203 well as the identification of chimeric junctions; and the machine-learning models
204 rely on supervised training with labeled examples, which may limit their ability
205 to detect novel or unexpected chimeric patterns.

206 1.5 Significance of the Research

207 This research provides both methodological and practical contributions to mito-
208 chondrial genomics and bioinformatics. First, MitoChime detects PCR-induced
209 chimeric reads prior to genome assembly, with the goal of improving the con-
210 tinuity and correctness of *Sardinella lemuru* mitochondrial assemblies. Second,
211 it replaces informal manual curation with a documented workflow, improving au-
212 tomation and reproducibility. Third, the pipeline is designed to run on computing
213 infrastructures commonly available in regional laboratories, enabling routine use
214 at facilities such as PGC Visayas. Finally, more reliable mitochondrial assemblies
215 for *S. lemuru* provide a stronger basis for downstream applications in the field of
216 fisheries and genomics.

²¹⁷ **Chapter 2**

²¹⁸ **Review of Related Literature**

²¹⁹ This chapter presents an overview of the literature relevant to the study. It
²²⁰ discusses the biological and computational foundations underlying mitochondrial
²²¹ genome analysis and assembly, as well as existing tools, algorithms, and techniques
²²² related to chimera detection and genome quality assessment. The chapter aims to
²²³ highlight the strengths, limitations, and research gaps in current approaches that
²²⁴ motivate the development of the present study.

²²⁵ **2.1 The Mitochondrial Genome**

²²⁶ Mitochondrial genome (mtDNA) is a small, typically circular molecule found in
²²⁷ most eukaryotes. It encodes essential genes involved in oxidative phosphorylation
²²⁸ and energy metabolism. Because of its conserved structure, mtDNA has become
²²⁹ a valuable genetic marker for studies in population genetics and phylogenetics
²³⁰ (Anderson et al., 1981; Boore, 1999). In animal species, the mitochondrial genome

ranges from 15–20 kilobase and contains 13 protein-coding genes, 22 tRNAs, and two rRNAs arranged compactly without introns (Gray, 2012). In comparison to nuclear DNA, the ratio of the number of copies of mtDNA is higher and has simple organization which make it particularly suitable for genome sequencing and assembly studies (Dierckxsens et al., 2017).

2.1.1 Mitochondrial Genome Assembly

Mitochondrial genome assembly refers to the reconstruction of the complete mitochondrial DNA (mtDNA) sequence from raw or fragmented sequencing reads. It is conducted to obtain high-quality, continuous representations of the mitochondrial genome that can be used for a wide range of analyses, including species identification, phylogenetic reconstruction, evolutionary studies, and investigations of mitochondrial diseases. Because mtDNA evolves rapidly, its assembled sequence provides valuable insights into population structure, lineage divergence, and adaptive evolution across taxa (Boore, 1999). Compared to nuclear genome assembly, assembling the mitochondrial genome is often considered more straightforward but still encounters technical challenges such as the formation of chimeric reads. Commonly used tools for mitogenome assembly such as GetOrganelle and MITObim operate under the assumption of organelle genome circularity, and are vulnerable when chimeric reads disrupt this circular structure, resulting in assembly errors (Hahn et al., 2013; Jin et al., 2020).

251 2.2 PCR Amplification and Chimera Formation

252 PCR plays an important role in NGS library preparation, as it amplifies target
253 DNA fragments for downstream analysis. However as previously mentioned, the
254 amplification process can also introduce chimeric reads which compromises the
255 quality of the input reads supplied to sequencing or assembly workflows. Chimeras
256 typically arise when incomplete extension occurs during a PCR cycle. This causes
257 the DNA polymerase to switch from one template to another and generate hy-
258 brid recombinant molecules (Judo et al., 1998). Artificial chimeras are produced
259 through such amplification errors, whereas biological chimeras occur naturally
260 through genomic rearrangements or transcriptional events.

261 In the context of amplicon-based sequencing, the presence of chimeras can in-
262 flate estimates of genetic or microbial diversity and may cause misassemblies dur-
263 ing genome reconstruction. Qin et al. (2023) has reported that chimeric sequences
264 may account for more than 10% of raw reads in amplicon datasets. This artifact
265 tends to be most prominent among rare operational taxonomic units (OTUs) or
266 singletons, which are sometimes misinterpreted as novel diversity, further caus-
267 ing the complication of microbial diversity analyses (Gonzalez, Zimmermann, &
268 Saiz-Jimenez, 2004). As such, determining and minimizing PCR-induced chimera
269 formation is vital for improving the quality of mitochondrial genome assemblies,
270 and ensuring the reliability of amplicon sequencing data.

271 **2.3 Existing Traditional Approaches for Chimera**

272 **Detection**

273 Several computational tools have been developed to identify chimeric sequences in
274 NGS datasets. These tools generally fall into two categories: reference-based and
275 de novo approaches. Reference-based chimera detection, also known as database-
276 dependent detection, is one of the earliest and most widely used computational
277 strategies for identifying chimeric sequences in amplicon-based community studies.
278 These methods rely on the comparison of each query sequence against a curated,
279 high-quality database of known, non-chimeric reference sequences (Edgar et al.,
280 2011).

281 On the other hand, the de novo chimera detection, also referred to as reference-
282 free detection, represents an alternative computational paradigm that identifies
283 chimeric sequences without reliance on external reference databases. This method
284 infer chimeras based on internal relationships among the sequences present within
285 the dataset itself, making it particularly advantageous in studies of under explored
286 or taxonomically diverse communities where comprehensive reference databases
287 are unavailable or incomplete (Edgar, 2016; Edgar et al., 2011). The underlying
288 assumption on this method is that during PCR, true biological sequences are
289 generally more abundant as they are amplified early and dominate the read pool,
290 whereas chimeric sequences appear later and are generally less abundant. The
291 de novo approach leverage this abundance hierarchy, treating the most abundant
292 sequences as supposed parents and testing whether less abundant sequences can
293 be reconstructed as mosaics of these templates. Compositional and structural
294 similarity are also evaluated to check whether different regions of a candidate

295 sequence correspond to distinct high-abundance sequences.

296 In practice, many modern bioinformatics pipelines combine both paradigms
297 sequentially: an initial de novo step identifies dataset-specific chimeras, followed
298 by a reference-based pass that removes remaining artifacts relative to established
299 databases (Edgar, 2016). These two methods of detection form the foundation of
300 tools such as UCHIME and later UCHIME2.

301 2.3.1 UCHIME

302 UCHIME is one of the most widely used tools for detecting chimeric sequences in
303 amplicon-based studies and remains a standard quality-control step in microbial
304 community analysis. Its core strategy is to test whether a query sequence (Q) can
305 be explained as a mosaic of two parent sequences, (A and B), and to score this
306 relationship using a structured alignment model (Edgar et al., 2011).

307 In reference mode, UCHIME divides the query into several segments and maps
308 them against a curated database of non-chimeric sequences. Candidate parents
309 are identified, and a three-way alignment is constructed. The algorithm assigns
310 “Yes” votes when different segments of the query match different parents and
311 “No” votes when the alignment contradicts a chimeric pattern. The final score
312 reflects the balance of these votes. In de novo mode, UCHIME operationalizes the
313 abundance-skew principle described earlier: high-abundance sequences are treated
314 as candidate parents, and lower-abundance sequences are evaluated as potential
315 mosaics. This makes the method especially useful when no reliable reference
316 database exists.

317 Although UCHIME is highly sensitive, it faces key constraints. Chimeras
318 formed from parents with very low divergence (below 0.8%) are difficult to detect
319 because they are nearly indistinguishable from sequencing errors. Accuracy in ref-
320 erence mode depends strongly on database completeness, while de novo detection
321 assumes that true parents are both present and sufficiently more abundant, such
322 conditions are not always met.

323 **2.3.2 UCHIME2**

324 UCHIME2 extends the original algorithm with refinements tailored for high-
325 resolution sequencing data. One of its major contributions is a re-evaluation
326 of benchmarking practices. Edgar (2016) demonstrated that earlier accuracy es-
327 timates for chimera detection were overly optimistic because they relied on un-
328 realistic scenarios where all true parent sequences were assumed to be present.
329 Using the more rigorous CHSIMA benchmark, UCHIME2 showed the prevalence
330 of “fake models” or real biological sequences that can be perfectly reconstructed
331 as apparent chimeras of other sequences, which suggests that perfect chimera de-
332 tection is theoretically unattainable. UCHIME2 also introduces several preset
333 modes (e.g., denoised, balanced, sensitive, specific, high-confidence) designed to
334 tune sensitivity and specificity depending on dataset characteristics. These modes
335 allow users to adjust the algorithm to the expected noise level or analytical goals.

336 Despite these improvements, UCHIME2 must be applied with caution. The
337 author’s website manual (Edgar, n.d) explicitly advises against using UCHIME2
338 as a standalone chimera-filtering step in OTU clustering or denoising workflows
339 because doing so can inflate both false positives and false negatives.

340 **2.3.3 CATch**

341 As previously mentioned, UCHIME (Edgar et al., 2011) relied on alignment-based
342 sequences in amplicon data. However, researchers soon observed that different al-
343 gorithms often produced inconsistent predictions. A sequence might be identified
344 as chimeric by one tool but classified as non-chimeric by another, resulting in
345 unreliable filtering outcomes across studies.

346 To address these inconsistencies, Mysara, Saeys, Leys, Raes, and Monsieurs
347 (2015) developed the Classifier for Amplicon Tool Chimeras (CATCh), which rep-
348 resents the first ensemble machine learning system designed for chimera detection
349 in 16S rRNA amplicon sequencing. Rather than depending on a single detec-
350 tion strategy, CATCh integrates the outputs of several established tools, includ-
351 ing UCHIME, ChimeraSlayer, DECIPHER, Pintail, and Perseus. The individual
352 scores and binary decisions generated by these tools are used as input features for
353 a supervised learning model. The algorithm employs a Support Vector Machine
354 (SVM) with a Pearson VII Universal Kernel (PUK) to determine optimal weight-
355 ings among the input features and to assign each sequence a probability of being
356 chimeric.

357 Benchmarking in both reference-based and de novo modes demonstrated signif-
358 icant performance improvements. CATCh achieved sensitivities of approximately
359 85 percent in reference-based mode and 92 percent in de novo mode, with corre-
360 sponding specificities of approximately 96 percent and 95 percent. These results
361 indicate that CATCh detected 7 to 12 percent more chimeras than any individual
362 algorithm while maintaining high precision.

363 **2.3.4 ChimPipe**

364 Among the available tools for chimera detection, ChimPipe is a pipeline developed
365 to identify chimeric sequences such as biological chimeras. It uses both discordant
366 paired-end reads and split-read alignments to improve the accuracy and sensitivity
367 of detecting biological chimeras (Rodriguez-Martin et al., 2017). By combining
368 these two sources of information, ChimPipe achieves better precision than meth-
369 ods that depend on a single type of indicator.

370 The pipeline works with many eukaryotic species that have available genome
371 and annotation data (Rodriguez-Martin et al., 2017). It can also predict multiple
372 isoforms for each gene pair and identify breakpoint coordinates that are useful
373 for reconstructing and verifying chimeric transcripts. Tests using both simulated
374 and real datasets have shown that ChimPipe maintains high accuracy and reliable
375 performance.

376 ChimPipe lets users adjust parameters to fit different sequencing protocols or
377 organism characteristics. Experimental results have confirmed that many chimeric
378 transcripts detected by the tool correspond to functional fusion proteins, demon-
379 strating its utility for understanding chimera biology and its potential applications
380 in disease research (Rodriguez-Martin et al., 2017).

381 2.4 Machine Learning Approaches for Chimera 382 and Sequence Quality Detection

383 Traditional chimera detection tools rely primarily on heuristic or alignment-based
384 rules. Recent advances in machine learning (ML) have demonstrated that models
385 trained on sequence-derived features can effectively capture compositional and
386 structural patterns in biological sequences. Although most existing ML systems
387 such as those used for antibiotic resistance prediction, taxonomic classification,
388 or viral identification are not specifically designed for chimera detection, they
389 highlight how data-driven models can outperform similarity-based heuristics by
390 learning intrinsic sequence signatures. In principle, ML frameworks can integrate
391 indicators such as k-mer frequencies, GC-content variation and split-alignment
392 metrics to identify subtle anomalies that may indicate a chimeric origin (Arango
393 et al., 2018; Liang, Bible, Liu, Zou, & Wei, 2020; Ren et al., 2020).

394 2.4.1 Feature-Based Representations of Genomic Sequences

396 Feature extraction converts DNA sequences into numerical representations suit-
397 able for machine-learning models. One approach is k-mer frequency analysis,
398 which counts short nucleotide sequences within a read (Vervier, Mahé, Tournoud,
399 Veyrieras, & Vert, 2015). High-frequency k-mers, including simple repeats such
400 as “AAAAAA,” can highlight repetitive or unusual regions that may occur near
401 chimeric junctions. Comparing k-mer patterns across adjacent parts of a read can
402 help identify such regions, while GC content provides an additional descriptor of

403 local sequence composition (Ren et al., 2020).

404 Alignment-derived features further inform junction detection. Long-read tools
405 such as Sniffles (Sedlazeck et al., 2018) use split alignments to locate breakpoints
406 across extended sequences, whereas short-read aligners like Minimap2 (Li, 2018)
407 report supplementary and secondary alignments that indicate local discontinu-
408 ities. Split alignments, where parts of a read map to different regions, can reveal
409 template-switching events. These features complement k-mer profiles and en-
410 hance detection of potentially chimeric reads, even in datasets with incomplete
411 references.

412 Microhomology, or short sequences shared between adjacent segments, is an-
413 other biologically meaningful feature. Its length, typically a few to tens of base
414 pairs, has been linked to microhomology-mediated repair and template-switching
415 mechanisms (Sfeir & Symington, 2015). In PCR-induced chimeras, short iden-
416 tical sequences at junctions provide a clear signature of chimerism. Measuring
417 the longest exact overlap at each breakpoint complements k-mer and alignment
418 features and helps identify reads that are potentially chimeric.

419 **2.5 Synthesis of Chimera Detection Approaches**

420 To provide an integrated overview of the literature discussed in this chapter, Ta-
421 ble 2.1 summarizes the major chimera detection studies, their methodological
422 approaches, and their known limitations.

Table 2.1: Comparison of Chimera Detection Approaches and Tools

Method / Tool	Core Approach	Key Limitations
Reference-based Detection	Compares each query sequence against curated databases of verified, non-chimeric sequences; evaluates segment similarity to identify mosaic patterns.	Accuracy depends on database completeness; performs poorly for novel taxa or missing parents; limited sensitivity for low-divergence chimeras.
De novo Detection	Identifies chimeras using only internal dataset structure; leverages abundance hierarchy and compositional similarity to infer whether low-abundance sequences can be reconstructed from abundant parents.	Assumes true sequences are more abundant; fails when amplification bias distorts abundances; struggles when parental sequences are similarly abundant or highly similar.
UCHIME	Alignment-based model that partitions the query into segments, identifies parent candidates, and computes a chimera score via a three-way alignment; supports reference and de novo modes.	Reduced accuracy for very closely related parents (<0.8% divergence); sensitive to incomplete databases; de novo mode fails if parents are absent or not sufficiently more abundant.
UCHIME2	Updated UCHIME with improved benchmarking (CHSIMA) and multiple sensitivity/specificity presets; better handles incomplete references and dataset variability.	“Fake models” limit theoretical accuracy; genuine variants may mimic chimeras; not recommended as a standalone step in OTU or denoising pipelines due to increased false positives/negatives.
CATCh	First ensemble ML model for 16S chimera detection; integrates outputs of UCHIME, ChimeraSlayer, DECIPHER, Pintail, and Perseus using an SVM to boost overall prediction accuracy.	Performance constrained by underlying tools; ML model cannot capture features not present in component algorithms; may misclassify in highly novel or low-coverage datasets.
ChimPipe	Pipeline for detecting biological chimeras in RNA-seq using discordant paired-end reads and split-read alignments; identifies isoforms and breakpoint coordinates.	Requires high-quality genome and annotation; tailored to RNA-seq rather than amplicons; computationally intensive; limited to organisms with available reference genomes.

423 Across existing studies, no single approach reliably detects all forms of chimeric
424 sequences, and the reviewed literature consistently shows that chimeras remain a
425 persistent challenge in genomics and bioinformatics. Although the surveyed tools
426 are not designed specifically for organelle genome assembly, they provide valua-
427 ble insights into which methodological strategies are effective and where current
428 approaches fall short. These limitations collectively define a clear research gap:
429 the need for a specialized, feature-driven detection framework tailored to PCR-
430 induced mitochondrial chimeras. Addressing this gap aligns with the research
431 objective outlined in Section 1.3, which is to develop and evaluate a machine-
432 learning-based pipeline (MitoChime) that improves the quality of downstream
433 mitochondrial genome assembly. In support of this aim, the subsequent chapters
434 describe the design, implementation, and evaluation of the proposed tool.

⁴³⁵ Chapter 3

⁴³⁶ Research Methodology

⁴³⁷ This chapter outlines the steps involved in completing the study, including data
⁴³⁸ gathering, generating simulated mitochondrial Illumina reads, preprocessing and
⁴³⁹ indexing the data, developing a feature extraction pipeline to extract key features,
⁴⁴⁰ applying machine learning algorithms for chimera detection, and validating and
⁴⁴¹ comparing model performance.

⁴⁴² 3.1 Research Activities

⁴⁴³ As illustrated in Figure 3.1, this study carried out a sequence of procedures to
⁴⁴⁴ detect PCR-induced chimeric reads in mitochondrial genomes. The process began
⁴⁴⁵ with collecting a mitochondrial reference sequence of *Sardinella lemuru* from the
⁴⁴⁶ National Center for Biotechnology Information (NCBI) database, which was used
⁴⁴⁷ as a reference for generating simulated clean and chimeric reads. These reads
⁴⁴⁸ were subsequently indexed and mapped. The resulting collections then passed

449 through a feature extraction pipeline that extracted k-mer profiles, supplementary
450 alignment (SA) features, and microhomology information to prepare the data for
451 model construction. The machine learning model was trained using the processed
452 input, and its precision and accuracy were assessed. It underwent tuning until it
453 reached the desired performance threshold, after which it proceeded to validation
454 and will undergo testing.

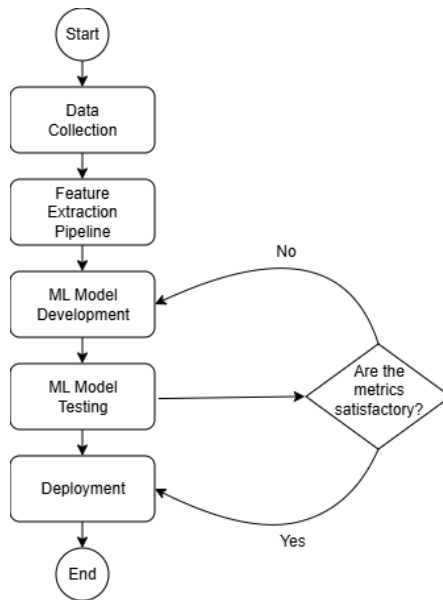


Figure 3.1: Process Diagram of Special Project

455 3.1.1 Data Collection

456 The mitochondrial genome reference sequence of *S. lemuru* was obtained from the
457 NCBI database (accession number NC_039553.1) in FASTA format. This sequence
458 served as the basis for generating simulated reads for model development.

459 This step was scheduled to begin in the first week of November 2025 and
460 expected to be completed by the end of that week, with a total duration of ap-

461 proximately one (1) week.

462 Data Preprocessing

463 To reduce manual repetition, all steps in the simulation and preprocessing pipeline
464 were executed using a custom script in Python (Version 3.11). The script runs
465 each stage, including read simulation, reference indexing, mapping, and alignment
466 processing, in a fixed sequence.

467 Sequencing data were simulated from the NCBI reference genome using `wgsim`
468 (Version 1.13). First, a total of 10,000 paired-end fragments were simulated,
469 producing 20,000 reads (10,000 forward and 10,000 reverse) from the the original
470 reference (`original_reference.fasta`) and and designated as clean reads using
471 the command:

```
472 wgsim -1 150 -2 150 -r 0 -R 0 -X 0 -e 0.001 -N 10000 \  
473     original_reference.fasta ref1.fastq ref2.fastq
```

474 The command parameters are as follows:

- 475 • `-1` and `-2`: read lengths of 150 base pairs for each paired-end read.
- 476 • `-r`, `-R`, `-X`: mutation rate, fraction of indels, and indel extension probability,
477 all set to a default value of 0.
- 478 • `-e`: base error rate, set to 0.001 to simulate realistic sequencing errors.
- 479 • `-N`: number of read pairs, set to 10,000.

480 Chimeric sequences were then generated from the same NCBI reference using a
481 separate Python script. Two non-adjacent segments were randomly selected such
482 that their midpoint distances fell within specified minimum and maximum thresh-
483 olds. The script attempts to retain microhomology, or short identical sequences
484 at segment junctions, to mimic PCR-induced template switching. The resulting
485 chimeras were written to `chimera_reference.fasta`, with headers recording seg-
486 ment positions and microhomology length. The `chimera_reference.fasta` was
487 processed with `wgsim` to simulate 10,000 paired-end fragments, generating 20,000
488 chimeric reads (10,000 forward reads in `chimeric1.fastq` and 10,000 reverse reads
489 in `chimeric2.fastq`) using the command format.

490 Next, a `minimap2` index of the reference genome was created using:

```
491 minimap2 -d ref.mmi original_reference.fasta
```

492 Minimap2 (Version 2.28) is a tool used to map reads to a reference genome.
493 The index `ref.mmi` of the original reference sequence is required by `minimap2` for
494 efficient read mapping. Mapping allows extraction of alignment features from each
495 read, which were used as input for the machine learning model. The simulated
496 clean and chimeric reads were then mapped to the reference index as follows:

```
497 minimap2 -ax sr -t 8 ref.mmi ref1.fastq ref2.fastq > clean.sam
```

```
498 minimap2 -ax sr -t 8 ref.mmi \  
499 chimeric1.fastq chimeric2.fastq > chimeric.sam
```

500 Here, `-ax sr` specifies short-read alignment mode, and `-t 8` uses 8 CPU

501 threads. The resulting clean and chimeric SAM files contain the alignment posi-
502 tions of each read relative to the original reference genome.

503 The SAM files were then converted to BAM format, sorted, and indexed using

504 `samtools` (Version 1.20):

```
505 samtools view -bS clean.sam -o clean.bam  
506 samtools view -bS chimeric.sam -o chimeric.bam  
507  
508 samtools sort clean.bam -o clean.sorted.bam  
509 samtools index clean.sorted.bam  
510  
511 samtools sort chimeric.bam -o chimeric.sorted.bam  
512 samtools index chimeric.sorted.bam
```

513 BAM files are the compressed binary version of SAM files, which enables faster
514 processing and reduced storage. Sorting arranges reads by genomic coordinates,
515 and indexing allows detection of SA as a feature for the machine learning model.

516 The total number of simulated reads was expected to be 40,000. The final col-
517 lection of reads contained 19,984 clean reads and 20,000 chimeric reads (39,984 en-
518 tries in total), providing a roughly balanced distribution between the two classes.
519 After alignment with `minimap2`, only 19,984 clean reads remained because un-
520 mapped reads were not included in the BAM file. Some sequences failed to align
521 due to the 5% error rate defined during `wgsim` simulation, which produced mis-
522 matches that caused certain reads to fall below the aligner's matching threshold.

523 This whole process is scheduled to start in the second week of November 2025

524 and is expected to be completed by the last week of November 2025, with a total
525 duration of approximately three (3) weeks.

526 3.1.2 Feature Extraction Pipeline

527 This stage directly follows the previous alignment phase, utilizing the resulting
528 BAM files (specifically `chimeric.sorted.bam` and `clean.sorted.bam`). A custom
529 Python script was created to efficiently process each primary-mapped read to
530 extract the necessary set of analytical features, which are then compiled into a
531 structured feature matrix in TSV format. The pipeline's core functionality relies
532 on libraries, namely `Pysam` (Version 0.22) for the robust parsing of BAM structures
533 and `NumPy` (Version 1.26) for array operations and computations. The pipeline
534 focuses on three principal features that collectively capture biological signatures
535 associated with PCR-induced chimeras: (1) Supplementary alignment flag (SA
536 count), (2) k-mer composition difference, and (3) microhomology.

537 Supplementary Alignment Flag

538 Split-alignment information was derived from the `SA` (Supplementary Alignment)
539 tag embedded in each primary read of the BAM file. This tag is typically asso-
540 ciated with reads that map to multiple genomic locations, suggesting a chimeric
541 structure. To extract this information, the script first checked whether the read
542 carried an `SA:Z` tag. If present, the tag string was parsed using the function
543 `parse_sa_tag`, yielding a structure for each alignment containing the reference
544 name, mapped position, strand, mapping quality, and number of mismatches.

545 After parsing, the function `sa_feature_stats` was applied to establish the fun-
546 damental split indicators, `has_sa` and `sa_count`. Along with these initial counts,
547 the function synthesized a summarization by aggregating metrics related to the
548 structure and reliability of the split alignments.

549 K-mer Composition Difference

550 Chimeric reads often comprise fragments from distinct genomic regions, resulting
551 in a compositional discontinuity between segments. Comparing k-mer frequency
552 profiles between the left and right halves of a read allows for the detection of such
553 abrupt compositional shifts, independent of alignment information.

554 The script implemented this by inferring a likely junction breakpoint using
555 the function `infer_breakpoints`, prioritizing the boundaries defined by soft-
556 clipping operations in the CIGAR string. If no clipping was present, the midpoint
557 of the alignment or the read length was utilized as a fallback. The read sequence
558 was then divided into left and right segments at this inferred breakpoint, and
559 k-mer frequency profiles ($k = 5$) were generated for both halves, ignoring any
560 k-mers containing ambiguous 'N' bases. The resulting k-mer frequency vectors
561 will be normalized and compared using the functions `cosine_difference` and
562 `js_divergence`.

563 Microhomology

564 The workflow for extracting the microhomology feature also started by utilizing
565 the `infer_breakpoints` similar to the k-mer workflow. Once a breakpoint was es-

566 established, the script scanned a ± 40 base pair window surrounding the breakpoint
567 and used the function `longest_suffix_prefix_overlap` to identify the longest
568 exact suffix-prefix overlap between the left and right read segments. This overlap,
569 which represents consecutive bases shared at the junction, was recorded as the
570 `microhomology_length` in the dataset. The 40-base pair window was chosen to
571 ensure that short shared sequences at or near the breakpoint were captured, with-
572 out including distant sequences that are unrelated. Additionally, the GC content
573 of the overlapping sequence was calculated using the function `gc_content`, which
574 counts guanine (G) and cytosine (C) bases within the detected microhomology
575 and divides by the total length, yielding a proportion between 0 and 1, and was
576 stored under the `microhomology_gc` attribute. Short microhomologies, typically
577 3-20 base pairs in length, are recognized signatures of PCR-induced template
578 switching (Peccoud et al., 2018).

579 A k-mer length of 6 was used to capture patterns within the same 40-base pair
580 window surrounding each breakpoint. These profiles complement microhomology
581 measurements and help identify junctions that are potentially chimeric.

582 To ensure correctness and adherence to best practices, bioinformatics experts
583 at the PGC Visayas will be consulted to validate the pipeline design, feature
584 extraction logic, and overall data integrity. This stage of the study was scheduled
585 to begin in the third week of November 2025 and conclude by the first week
586 of December 2025, with an estimated total duration of approximately three (3)
587 weeks.

588 **3.1.3 Machine Learning Model Development**

589 After feature extraction, the per-read feature matrices for clean and chimeric
590 reads were merged into a single dataset. Each row corresponded to one paired-
591 end read, and columns encoded alignment-structure features (e.g., supplementary
592 alignment count and spacing between segments), CIGAR-derived soft-clipping
593 statistics (e.g., left and right soft-clipped length, total clipped bases), k-mer com-
594 position discontinuity between read segments, and microhomology descriptors
595 near candidate junctions. The resulting feature set was restricted to quantities
596 that can be computed from standard BAM/FASTQ files in typical mitochondrial
597 sequencing workflows.

598 The labelled dataset was randomly partitioned into training (80%) and test
599 (20%) subsets using stratified sampling to preserve the 1:1 ratio of clean to
600 chimeric reads. Model development and evaluation were implemented in Python
601 (Version 3.11) using the `scikit-learn`, `xgboost`, `lightgbm`, and `catboost` li-
602 braries. A broad panel of classification algorithms was then benchmarked on the
603 training data to obtain a fair comparison of different model families under identical
604 feature conditions. The panel included: a trivial dummy classifier, L2-regularized
605 logistic regression, a calibrated linear support vector machine (SVM), k -nearest
606 neighbours, Gaussian Naïve Bayes, decision-tree ensembles (Random Forest, Ex-
607 tremely Randomized Trees, and Bagging with decision trees), gradient boosting
608 methods (Gradient Boosting, XGBoost, LightGBM, and CatBoost), and a shallow
609 multilayer perceptron (MLP).

610 For each model, five-fold stratified cross-validation was performed on the train-
611 ing set. In every fold, four-fifths of the data were used for fitting and the remaining

612 one-fifth for validation. Mean cross-validation accuracy, precision, recall, F1-score
613 for the chimeric class, and area under the receiver operating characteristic curve
614 (ROC–AUC) were computed to summarize performance and rank candidate meth-
615 ods. This baseline screen allowed comparison of linear, probabilistic, neural, and
616 ensemble-based approaches and identified tree-based ensemble and boosting mod-
617 els as consistently strong performers relative to simpler baselines.

618 **3.1.4 Model Benchmarking, Hyperparameter Optimiza-
619 tion, and Evaluation**

620 Model selection and refinement proceeded in two stages. First, the cross-validation
621 results from the broad panel were used to identify a subset of competitive mod-
622 els for more detailed optimization. Specifically, ten model families were carried
623 forward: L2-regularized logistic regression, calibrated linear SVM, Random For-
624 est, ExtraTrees, Gradient Boosting, XGBoost, LightGBM, CatBoost, Bagging
625 with decision trees, and a shallow MLP. This subset spans both linear and non-
626 linear decision boundaries, but emphasizes ensemble and boosting methods, which
627 showed superior F1 and ROC–AUC in the initial benchmark.

628 Second, hyperparameter optimization was conducted for each of the ten se-
629 lected models using randomized search with five-fold stratified cross-validation
630 (`RandomizedSearchCV`). For tree-based ensembles, the search space included the
631 number of trees, maximum depth, minimum samples per split and leaf, and the
632 fraction of features considered at each split. For boosting methods, key hyper-
633 parameters such as the number of boosting iterations, learning rate, tree depth,
634 subsampling rate, and column subsampling rate were tuned. For the MLP, the

635 number and size of hidden layers, learning rate, and L_2 regularization strength
636 were varied. In all cases, the primary optimisation criterion was the F1-score of
637 the chimeric class, averaged across folds.

638 For each model family, the hyperparameter configuration with the highest
639 mean cross-validation F1-score was selected as the best-tuned estimator. These
640 tuned models were then refitted on the full training set and evaluated once on the
641 held-out test set to obtain unbiased estimates of performance. Test-set metrics in-
642 cluded accuracy, precision, recall, F1-score for the chimeric class, and ROC–AUC.
643 Confusion matrices and ROC curves were generated for the top-performing mod-
644 els to characterise common error modes, such as false negatives (missed chimeric
645 reads) and false positives (clean reads incorrectly labelled as chimeric). The final
646 model or small set of models for downstream interpretation was chosen based on
647 a combination of test-set F1-score, ROC–AUC, and practical considerations such
648 as model complexity and ease of deployment within a feature extraction pipeline.

649 **3.1.5 Feature Importance and Interpretation**

650 To relate model decisions to biologically meaningful signals, feature-importance
651 analyses were performed on the best-performing tree-based models. Two comple-
652 mentary approaches were used. First, built-in importance measures from ensemble
653 methods (e.g., split-based importances in Random Forest and Gradient Boosting)
654 were examined to obtain an initial ranking of features based on their contribution
655 to reducing impurity. Second, model-agnostic permutation importance was com-
656 puted on the test set by repeatedly permuting each feature column while keeping
657 all others fixed and measuring the resulting decrease in F1-score. Features whose

658 permutation led to a larger performance drop were interpreted as more influential
659 for chimera detection.

660 For interpretability, individual features were grouped into four conceptual
661 families: (i) supplementary alignment and alignment-structure features (e.g., SA
662 count, spacing between alignment segments, strand consistency), (ii) CIGAR-
663 derived soft-clipping features (e.g., left and right soft-clipped length, total clipped
664 bases), (iii) k-mer composition discontinuity features (e.g., cosine distance and
665 Jensen–Shannon divergence between k-mer profiles of read segments), and (iv) mi-
666 crohomology descriptors (e.g., microhomology length and local GC content around
667 putative breakpoints). Aggregating permutation importance scores within each
668 family allowed assessment of which biological signatures contributed most strongly
669 to the classifier’s performance. This analysis provided a basis for interpreting the
670 trained models in terms of known mechanisms of PCR-induced template switching
671 and for identifying which alignment- and sequence-derived cues are most informa-
672 tive for distinguishing chimeric from clean mitochondrial reads.

673 3.1.6 Validation and Testing

674 Validation will involve both internal and external evaluations. Internal valida-
675 tion was achieved through five-fold cross-validation on the training data to verify
676 model generalization and reduce variance due to random sampling. External vali-
677 dation will be achieved through testing on the 20% hold-out dataset derived from
678 the simulated reads, which will be an unbiased benchmark to evaluate how well
679 the trained models generalized to unseen data. All feature extraction and prepro-
680 cessing steps were performed using the same feature extraction pipeline to ensure

681 consistency and comparability across validation stages.

682 Comparative evaluation was performed across all candidate algorithms, in-
683 cluding a trivial dummy classifier, L2-regularized logistic regression, a calibrated
684 linear SVM, k-nearest neighbours, Gaussian Naïve Bayes, decision-tree ensembles,
685 gradient boosting methods, and a shallow MLP. This evaluation determined which
686 models demonstrated the highest predictive performance and computational effi-
687 ciency under identical data conditions. Their metrics were compared to identify
688 which algorithms were most suitable for further refinement.

689 **3.1.7 Documentation**

690 Comprehensive documentation was maintained throughout the study to ensure
691 transparency and reproducibility. All stages of the research, including data gath-
692 ering, preprocessing, feature extraction, model training, and validation, were sys-
693 tematically recorded in a `.README` file in the GitHub repository. For each ana-
694 lytical step, the corresponding parameters, software versions, and command line
695 scripts were documented to enable exact replication of results.

696 The repository structure followed standard research data management prac-
697 tices, with clear directories for datasets and scripts. Computational environments
698 were standardized using Conda, with an environment file (`environment.arm.yml`)
699 specifying dependencies and package versions to maintain consistency across sys-
700 tems.

701 For manuscript preparation and supplementary materials, Overleaf (L^AT_EX)
702 was used to produce publication-quality formatting and consistent referencing. f

₇₀₃ **3.2 Calendar of Activities**

₇₀₄ Table 3.1 presents the project timeline in the form of a Gantt chart, where each
₇₀₅ bullet point corresponds to approximately one week of planned activity.

Table 3.1: Timetable of Activities

Activities (2025)	Nov	Dec	Jan	Feb	Mar	Apr	May
Data Collection and Simulation	• • •						
Feature Extraction Pipeline	• •	•					
Machine Learning Development			• •	• • •	• • •	• •	
Testing and Validation						• •	• • •
Documentation	• • •	• • •	• • •	• • •	• • •	• • •	• • •

706 **Chapter 4**

707 **Results and Discussion**

708 **4.1 Descriptive Analysis of Features**

709 This chapter presents the performance of the proposed feature set and machine-
710 learning models for detecting PCR-induced chimeric reads in simulated mitochon-
711 drial Illumina data. We first describe the behaviour of the main features, then
712 compare baseline classifiers, assess the effect of hyperparameter tuning, and fi-
713 nally analyse feature importance in terms of individual variables and biologically
714 motivated feature families.

715 The final dataset contained 31,986 reads for training and 7,997 reads for test-
716 ing, with classes balanced (approximately 4,000 clean and 4,000 chimeric reads in
717 the test split).

718 4.1.1 Exploratory Data Analysis

719 An exploratory data analysis (EDA) was conducted on the extracted feature ma-
720 trix to characterize general patterns in the data and gain preliminary insight into
721 which variables might meaningfully contribute to classification. Histograms of
722 key features indicated that alignment-based variables showed clear class separa-
723 tion as chimeric reads have higher frequencies of split alignments and and no-
724 ticeably broader long-tailed distribution on soft-clipped regions (`softclip_left`
725 and `softclip_right`). In contrast, sequence-based variables such a microhomol-
726 ogy length and k-mer divergence displayed substantial overlap between classes,
727 suggesting more limited discriminative value. The complete set of histograms is
728 provided in Appendix 4.6.

729 As shown in Figure 4.1, the feature correlation heatmap shows that alignment-
730 derived variables form a strongly correlated cluster, whereas sequence-derived
731 measures show weak correlations with both the alignment-based features and with
732 one another. This heterogeneity indicates that no single feature family captures
733 all relevant signal sources.

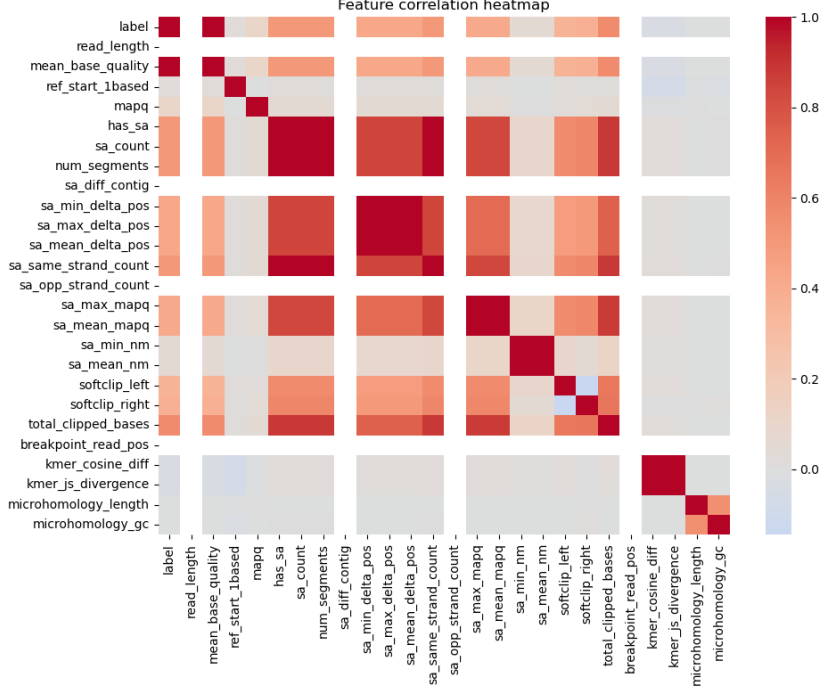


Figure 4.1: Feature correlation heatmap showing relationships among alignment-derived and sequence-derived variables.

734 4.2 Baseline Classification Performance

735 Table 4.1 summarises the performance of eleven classifiers trained on the engi-
 736 neered feature set using five-fold cross-validation and evaluated on the held-out
 737 test set. All models were optimised using default hyperparameters, without ded-
 738 icated tuning.

739 The dummy baseline, which always predicts the same class regardless of the
 740 input features, achieved an accuracy of 0.50 and test F1-score of 0.67. This re-
 741 flects the balanced class distribution and provides a lower bound for meaningful
 742 performance.

743 Across other models, test F1-scores clustered in a narrow band between ap-
 744 proximately 0.74 and 0.77 and ROC–AUC values between 0.82 and 0.84. Gradi-
 745 ent boosting, CatBoost, LightGBM, XGBoost, bagging trees, random forest, and
 746 multilayer perceptron (MLP) all produced very similar scores, with CatBoost and
 747 gradient boosting slightly ahead (test F1 \approx 0.77, ROC–AUC \approx 0.84). Linear
 748 models (logistic regression and calibrated linear SVM) performed only marginally
 749 worse (test F1 \approx 0.74), while Gaussian Naive Bayes lagged behind with substan-
 750 tially lower F1 (\approx 0.65) despite very high precision for the chimeric class.

Table 4.1: Performance of baseline classifiers on the held-out test set.

model	test_accuracy	test_precision	test_recall	test_f1	test_roc_auc
dummy_baseline	0.500000	0.500000	1.000000	0.667000	0.500000
logreg_l2	0.789000	0.945000	0.614000	0.744000	0.821000
linear_svm_calibrated	0.789000	0.945000	0.614000	0.744000	0.820000
random_forest	0.788000	0.894000	0.654000	0.755000	0.834000
extra_trees	0.788000	0.901000	0.647000	0.753000	0.824000
gradient_boosting	0.802000	0.936000	0.648000	0.766000	0.840000
xgboost	0.800000	0.929000	0.650000	0.765000	0.839000
lightgbm	0.799000	0.926000	0.650000	0.764000	0.838000
catboost	0.803000	0.936000	0.650000	0.767000	0.839000
knn	0.782000	0.892000	0.642000	0.747000	0.815000
gaussian_nb	0.741000	0.996000	0.483000	0.651000	0.819000
bagging_trees	0.792000	0.900000	0.657000	0.760000	0.837000
mlp	0.789000	0.931000	0.625000	0.748000	0.819000

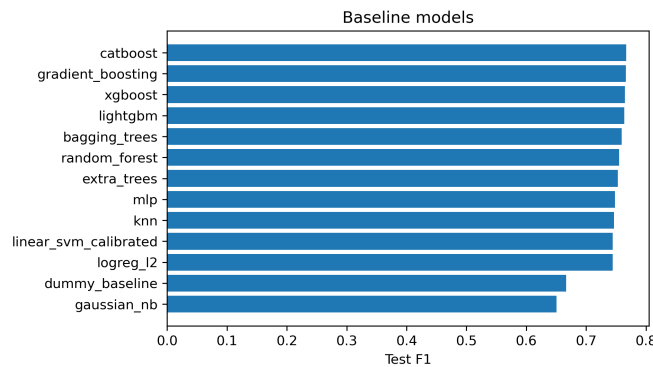


Figure 4.2: Test F1 of all baseline classifiers, showing that no single model clearly dominates and several achieve comparable performance.

751 4.3 Effect of Hyperparameter Tuning

752 To assess whether performance could be improved further, ten model families un-
753 derwent randomised hyperparameter search (Chapter 3). The tuned metrics are
754 summarised in Table 4.2. Overall, tuning yielded modest but consistent gains for
755 tree-based ensembles and boosting methods, while leaving linear models essen-
756 tially unchanged or slightly worse.

757 CatBoost, gradient boosting, LightGBM, XGBoost, random forest, bagging
758 trees, and MLP all experienced small increases in test F1 (typically $\Delta F1 \approx 0.002$ –
759 0.009) and ROC–AUC (up to $\Delta AUC \approx 0.008$). After tuning, CatBoost remained
760 the best performer with test accuracy 0.802, precision 0.924, recall 0.658, F1-score
761 0.769, and ROC–AUC 0.844. Gradient boosting achieved almost identical perfor-
762 mance (F1 0.767, AUC 0.843). Random forest and bagging trees also improved
763 to F1 scores around 0.763 with AUC ≈ 0.842 .

Table 4.2: Performance of tuned classifiers on the held-out test set.

model	test_accuracy	test_precision	test_recall	test_f1	test_roc_auc
logreg_l2_tuned	0.788000	0.946000	0.612000	0.743000	0.818000
linear_svm_calibrated_tuned	0.788000	0.944000	0.612000	0.743000	0.818000
random_forest_tuned	0.797000	0.915000	0.655000	0.763000	0.842000
extra_trees_tuned	0.794000	0.910000	0.652000	0.760000	0.837000
gradient_boosting_tuned	0.802000	0.928000	0.654000	0.767000	0.843000
xgboost_tuned	0.799000	0.922000	0.653000	0.765000	0.839000
lightgbm_tuned	0.801000	0.930000	0.651000	0.766000	0.842000
catboost_tuned	0.802000	0.924000	0.658000	0.769000	0.844000
bagging_trees_tuned	0.798000	0.922000	0.650000	0.763000	0.842000
mlp_tuned	0.790000	0.934000	0.625000	0.749000	0.821000

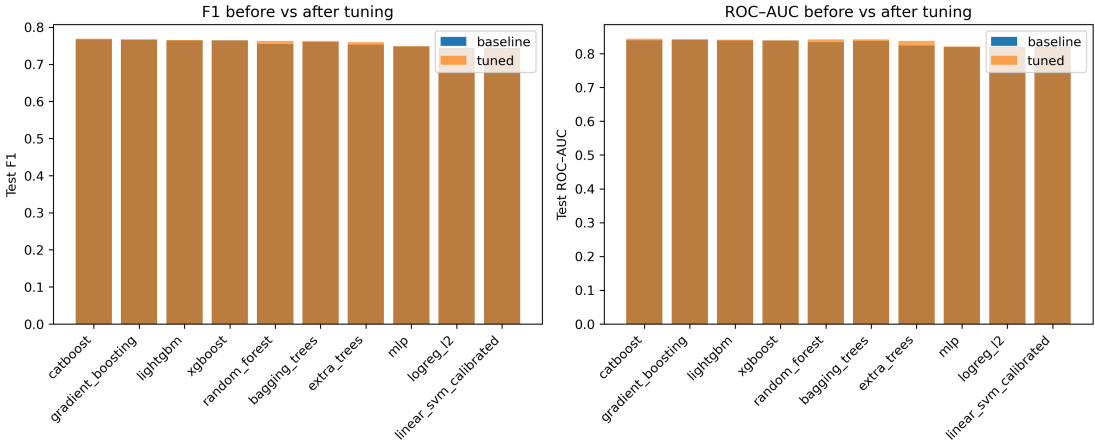


Figure 4.3: Comparison of test F1 (left) and ROC–AUC (right) for baseline and tuned models. Hyperparameter tuning yields small but consistent gains, particularly for tree-based ensembles.

764 Because improvements are small and within cross-validation variability, we
 765 interpret tuning as stabilising and slightly refining the models rather than funda-
 766 mentally altering their behaviour or their relative ranking.

767 4.4 Detailed Evaluation of Representative Mod- 768 els

769 For interpretability and diversity, four tuned models were selected for deeper
 770 analysis: CatBoost (best-performing boosted tree), scikit-learn gradient boost-
 771 ing (canonical gradient-boosting implementation), random forest (non-boosted
 772 ensemble baseline), and L2-regularised logistic regression (linear baseline). All
 773 models were trained on the engineered feature set and evaluated on the same
 774 held-out test data.

775 4.4.1 Confusion Matrices and Error Patterns

776 Classification reports and confusion matrices for the four models reveal consistent
777 patterns. CatBoost and gradient boosting both reached overall accuracy of ap-
778 proximately 0.80 with similar macro-averaged F1 scores (~ 0.80). For CatBoost,
779 precision and recall for clean reads were 0.73 and 0.95, respectively, while for
780 chimeric reads they were 0.92 and 0.66 ($F1 = 0.77$). Gradient boosting showed
781 nearly identical trade-offs.

782 Random forest attained slightly lower accuracy (0.80) and chimeric F1 (0.76),
783 whereas logistic regression achieved the lowest accuracy among the four (0.79)
784 and chimeric F1 (0.74), although it provided the highest chimeric precision (0.95)
785 at the cost of lower recall (0.61).

786 Across all models, errors were asymmetric. False negatives (chimeric reads
787 predicted as clean) were more frequent than false positives. For example, CatBoost
788 misclassified 1 369 chimeric reads as clean but only 215 clean reads as chimeric.
789 This pattern indicates that the models are conservative: they prioritise avoiding
790 spurious chimera calls at the expense of missing some true chimeras. Depending on
791 downstream application, alternative decision thresholds or cost-sensitive training
792 could be explored to adjust this balance.

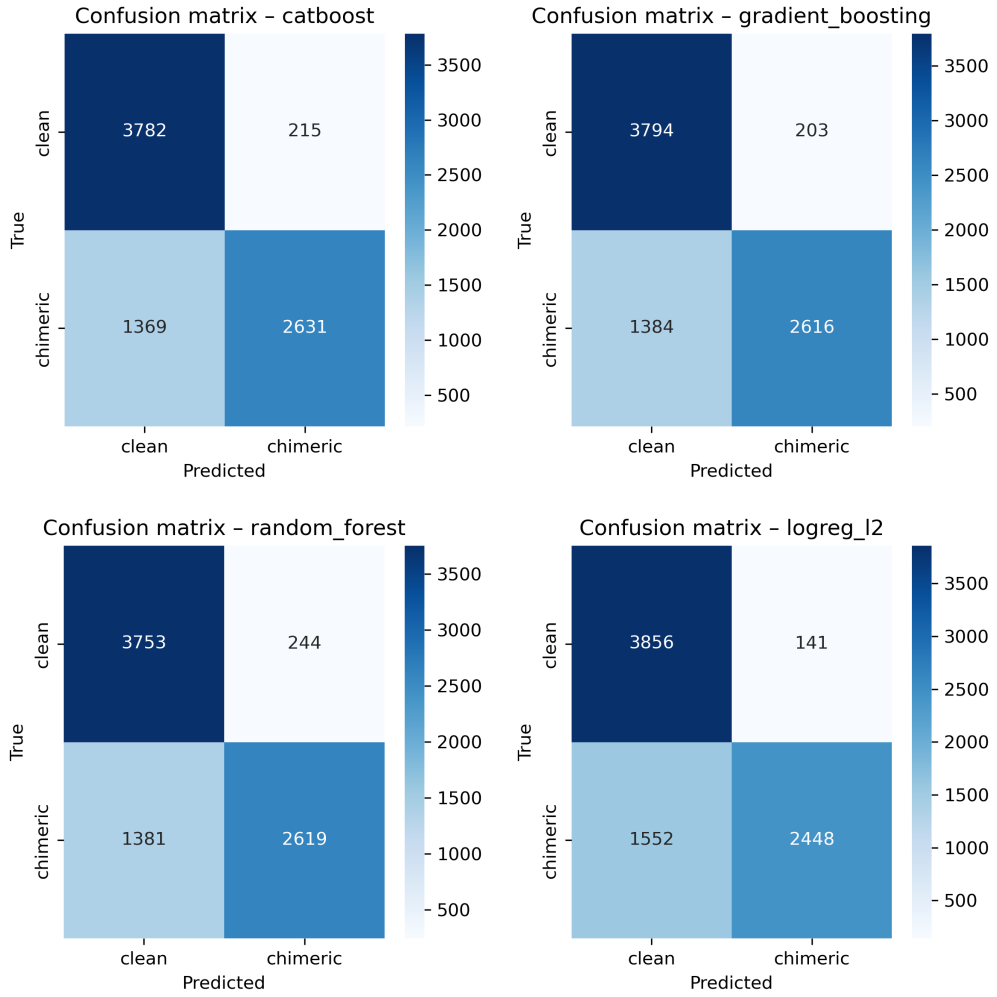


Figure 4.4: Confusion matrices for the four representative models on the held-out test set. All models show more false negatives (chimeric reads called clean) than false positives.

⁷⁹³ 4.4.2 ROC and Precision–Recall Curves

⁷⁹⁴ Receiver operating characteristic (ROC) and precision–recall (PR) curves (Figure 4.5) further support the similarity among the top models. The three tree-based
⁷⁹⁵ ensembles (CatBoost, gradient boosting, random forest) achieved ROC–AUC val-
⁷⁹⁶ ues of approximately 0.84 and average precision (AP) around 0.88. Logistic re-

798 gression performed slightly worse ($AUC \approx 0.82$, $AP \approx 0.87$) but still substantially
799 better than random guessing.

800 The PR curves show that precision remains above 0.9 across a broad range
801 of recall values (up to roughly 0.5–0.6), after which precision gradually declines.
802 This behaviour indicates that the models can assign very high confidence to a
803 subset of chimeric reads, while more ambiguous reads can only be recovered by
804 accepting lower precision.

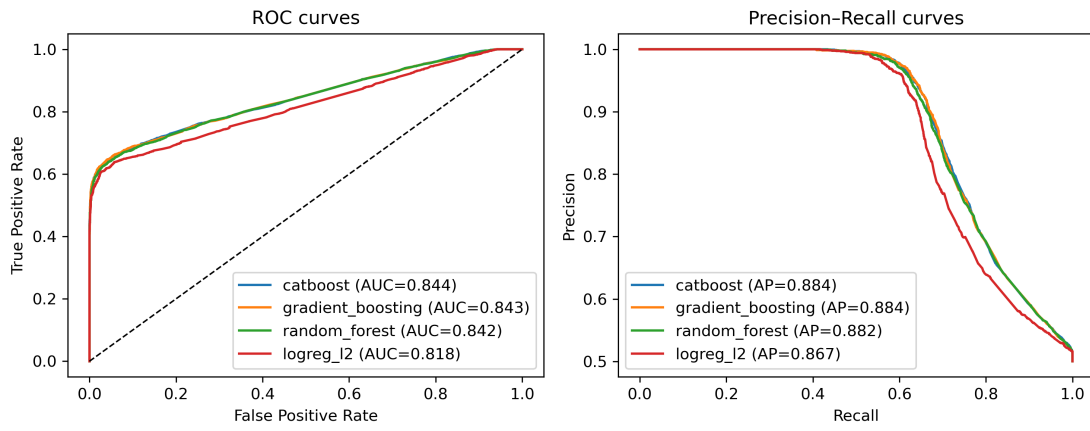


Figure 4.5: ROC (left) and precision–recall (right) curves for the four representative models on the held-out test set. Tree-based ensembles cluster closely, with logistic regression performing slightly but consistently worse.

805 **4.5 Feature Importance and Biological Interpre-**
806 **tation**

807 **4.5.1 Permutation Importance of Individual Features**

808 To understand how each classifier made predictions, feature importance was quan-
809 tified using permutation importance. In this approach, the values of a single fea-
810 ture are randomly shuffled, and the resulting drop in F_1 score (ΔF_1) reflects how
811 strongly the model depends on that feature. Greater decreases in F_1 indicate
812 stronger reliance on that feature. This analysis was applied to four representa-
813 tive models: CatBoost, Gradient Boosting, Random Forest, and L_2 -regularized
814 Logistic Regression.

815 As shown in Figure 4.6, the total number of clipped bases consistently pro-
816 vides a strong predictive signal, particularly in Random Forest, Gradient Boosting,
817 and L_2 -regularized Logistic Regression. CatBoost differs by assigning the highest
818 importance to k-mer divergence metrics such as `kmer_js_divergence`, which cap-
819 ture subtle sequence changes resulting from structural variants or PCR-induced
820 chimeras. Soft-clipping features (`softclip_left` and `softclip_right`) provide
821 additional context around breakpoints, complementing these primary signals in
822 all models except Gradient Boosting. L_2 -regularized Logistic Regression relies
823 more on alignment-based split-read metrics when breakpoints are simple, but it is
824 less effective at detecting complex rearrangements that introduce novel sequences.

825 Overall, these results indicate that accurate detection of chimeric reads relies
826 on both alignment-based signals and k-mer compositional information. Explicit

827 microhomology features contribute minimally in this analysis, and combining both
 828 alignment-based and sequence-level features enhances model sensitivity and speci-
 829 ficity.

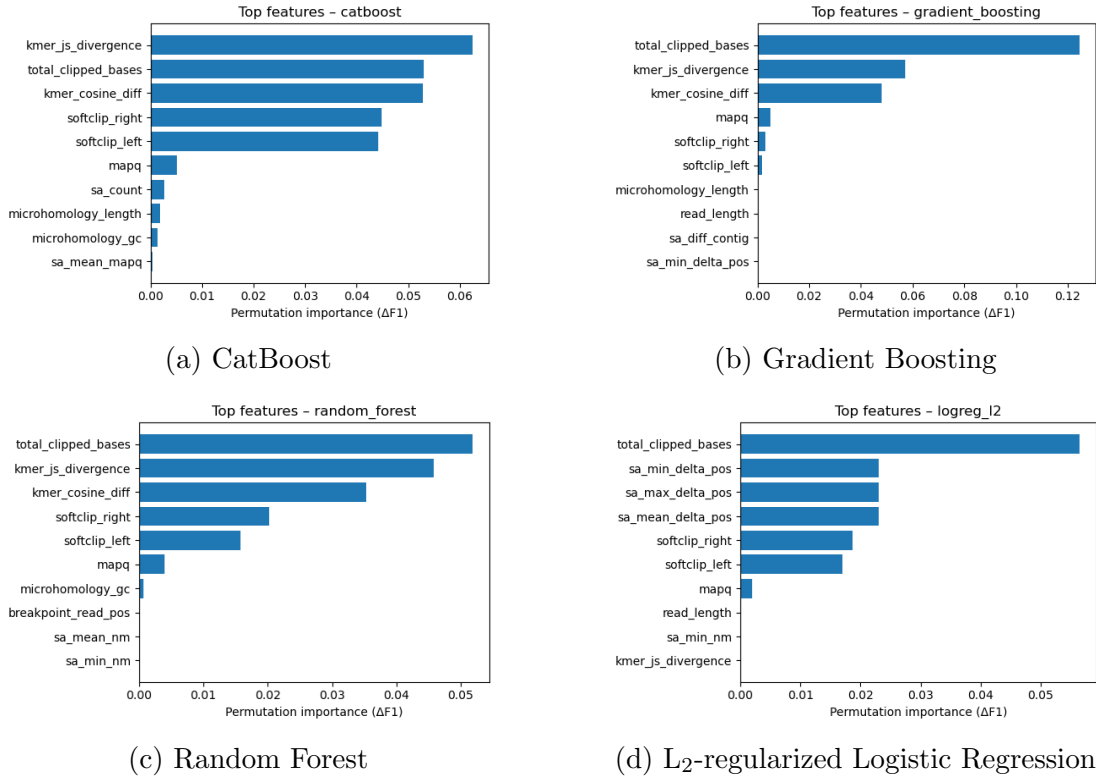


Figure 4.6: Permutation-based feature importance for four representative classifiers. Clipping and k-mer composition features are generally the strongest predictors, whereas microhomology and other alignment metrics contribute minimally.

830 4.5.2 Feature Family Importance

831 To evaluate the contribution of broader biological signals, features were
 832 grouped into five families: SA_structure (supplementary alignment and seg-
 833 ment metrics, e.g., has_sa, sa_count, sa_min_delta_pos, sa_mean_nm), Clipping
 834 (softclip_left, softclip_right, total_clipped_bases, breakpoint_read_pos),

835 Kmer_jump (`kmer_cosine_diff`, `kmer_js_divergence`), Micro_homology, and
836 Other (e.g., `mapq`).

837 Aggregated analyses reveal consistent patterns across models. In CatBoost,
838 the Clipping family has the largest cumulative contribution (0.14), followed
839 by Kmer_jump (0.12), with Other features contributing modestly (0.005) and
840 SA_structure (0.003) and Micro_homology (0.003) providing minimal predictive
841 power. Gradient Boosting shows a similar trend, with Clipping (0.13) domi-
842 nating, Kmer_jump (0.11) secondary, and the remaining families contributing
843 negligibly. Random Forest integrates both Clipping (0.088) and Kmer_jump
844 (0.08) effectively, while SA_structure, Micro_homology, and Other remain minor
845 contributors. L₂-regularized Logistic Regression emphasizes Clipping (0.09)
846 and SA_structure (0.07), with Kmer_jump and Micro_homology having minimal
847 impact.

848 Both feature-level and aggregated analyses indicate that detection of chimeric
849 reads in this dataset relies primarily on alignment disruptions (Clipping) and
850 k-mer compositional shifts (Kmer_jump), which often arise from PCR-induced
851 recombination events, while explicit microhomology features contribute minimally.

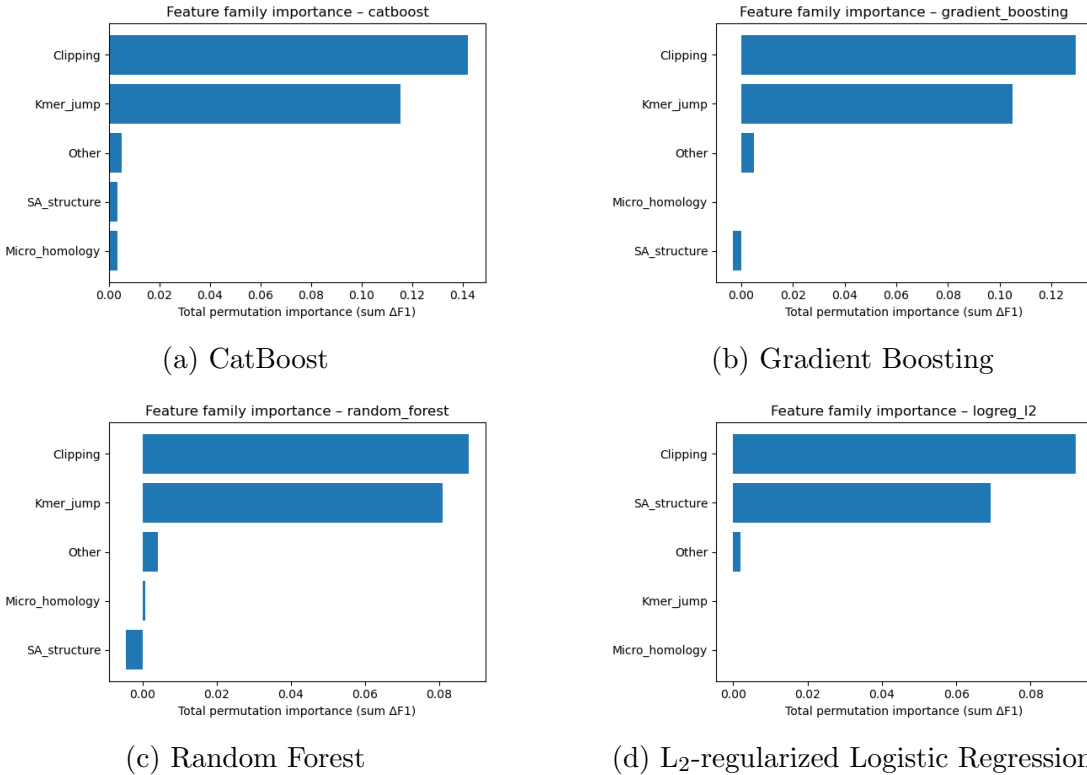


Figure 4.7: Aggregated feature family importance across four models. Clipping and k-mer compositional shifts are consistently the dominant contributors, while SA_structure, Micro_homology, and other features contribute minimally.

852 4.6 Summary of Findings

853 After removing trivially discriminative metadata, all models performed substan-
 854 tially better than the dummy baseline, with test F1-scores around 0.76 and ROC-
 855 AUC values near 0.84. Hyperparameter tuning yielded modest improvements,
 856 with boosting methods, particularly CatBoost and gradient boosting, achieving
 857 the highest performance. Confusion matrices and precision-recall curves indicate
 858 that these models prioritise precision for chimeric reads while accepting lower re-
 859 call, which a conservative strategy appropriate for scenarios where false positives

860 are costly.

861 Feature importance analyses revealed that alignment disruptions, such as clip-
862 ping, and abrupt k-mer composition changes accounted for most predictive power.
863 In contrast, microhomology metrics and supplementary alignment descriptors con-
864 tributed minimally. These results indicate that features based on read alignment
865 and k-mer composition are sufficient to train classifiers for detecting mitochon-
866 drial PCR-induced chimera reads, without needing additional quality-score or
867 positional information in the conditions tested.

⁸⁶⁸ **Appendix A**

⁸⁶⁹ **Histograms of Key Features**

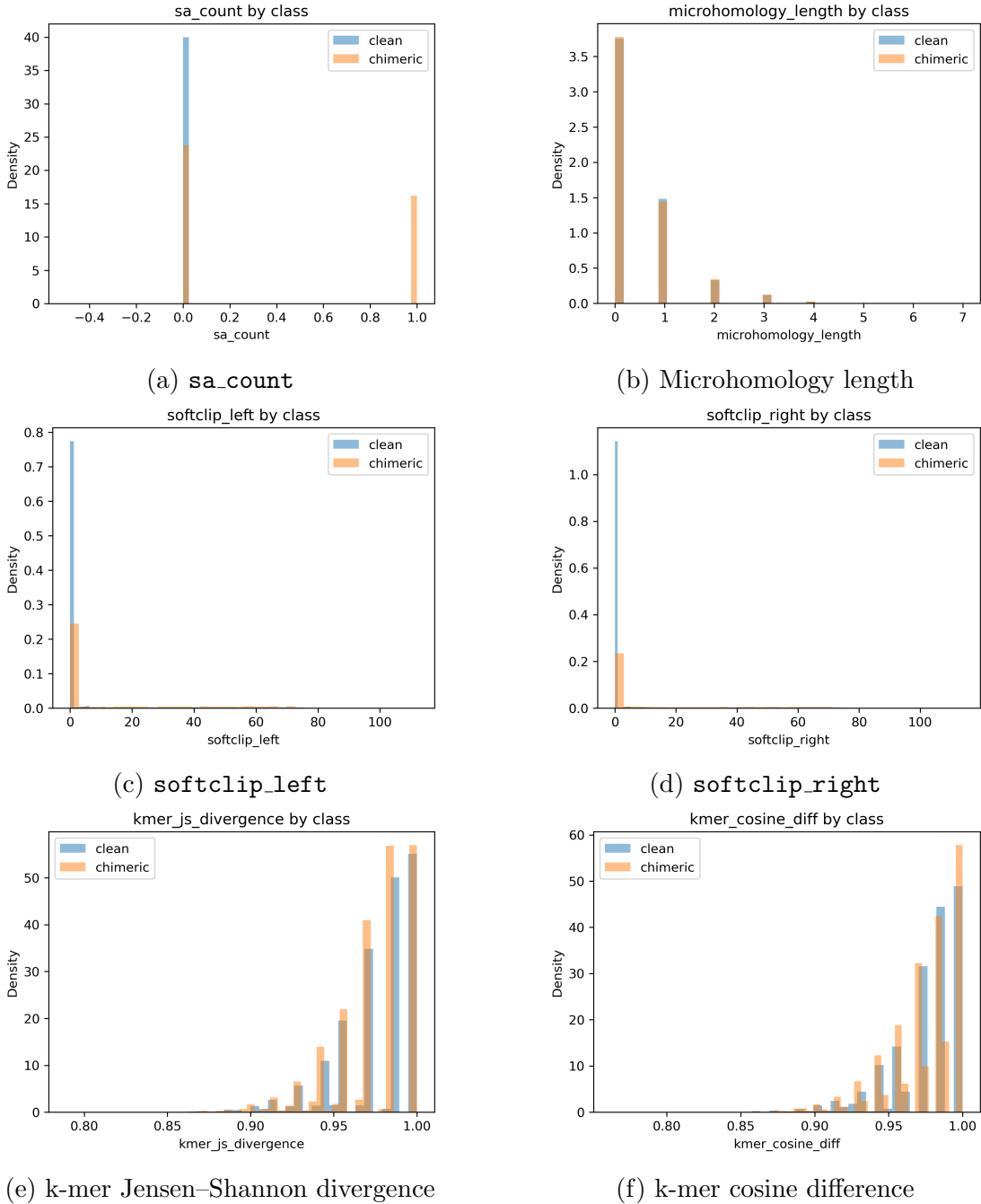


Figure A.1: Histogram plots of six key features comparing clean and chimeric reads.

870 References

- 871 Anderson, S., Bankier, A., Barrell, B., Bruijn, M., Coulson, A., Drouin, J., ...
872 Young, I. (1981, 04). Sequence and organization of the human mitochondrial
873 genome. *Nature*, *290*, 457-465. doi: 10.1038/290457a0
- 874 Arango, G., Garner, E., Pruden, A., Heath, L., Vikesland, P., & Zhang, L. (2018,
875 02). Deeparg: A deep learning approach for predicting antibiotic resistance
876 genes from metagenomic data. *Microbiome*, *6*. doi: 10.1186/s40168-018
877 -0401-z
- 878 Bentley, D. R., Balasubramanian, S., Swerdlow, H. P., Smith, G. P., Milton, J.,
879 Brown, C. G., ... Smith, A. J. (2008). Accurate whole human genome
880 sequencing using reversible terminator chemistry. *Nature*, *456*(7218), 53–
881 59. doi: 10.1038/nature07517
- 882 Boore, J. L. (1999). Animal mitochondrial genomes. *Nucleic Acids Research*,
883 *27*(8), 1767–1780. doi: 10.1093/nar/27.8.1767
- 884 Cameron, S. L. (2014). Insect mitochondrial genomics: Implications for evolution
885 and phylogeny. *Annual Review of Entomology*, *59*, 95–117. doi: 10.1146/
886 annurev-ento-011613-162007
- 887 Dierckxsens, N., Mardulyn, P., & Smits, G. (2017). Novoplasty: de novo assembly
888 of organelle genomes from whole genome data. *Nucleic Acids Research*,

- 889 45(4), e18. doi: 10.1093/nar/gkw955
- 890 Edgar, R. C. (2016). Uchime2: improved chimera prediction for amplicon se-
891 quencing. *bioRxiv*. Retrieved from <https://api.semanticscholar.org/>
892 CorpusID:88955007
- 893 Edgar, R. C. (n.d.). *Uchime in practice*. Retrieved from https://www.drive5.com/usearch/manual7/uchime_practical.html
- 894 Edgar, R. C., Haas, B. J., Clemente, J. C., Quince, C., & Knight, R. (2011).
895 Uchime improves sensitivity and speed of chimera detection. *Bioinformatics*,
896 27(16), 2194–2200. doi: 10.1093/bioinformatics/btr381
- 897 Glenn, T. C. (2011). Field guide to next-generation dna sequencers. *Molecular
898 Ecology Resources*, 11(5), 759–769. doi: 10.1111/j.1755-0998.2011.03024.x
- 899 Gonzalez, J. M., Zimmermann, J., & Saiz-Jimenez, C. (2004, 09). Evalu-
900 ating putative chimeric sequences from pcr-amplified products. *Bioin-
901 formatics*, 21(3), 333-337. Retrieved from <https://doi.org/10.1093/bioinformatics/bti008> doi: 10.1093/bioinformatics/bti008
- 902 Gray, M. W. (2012). Mitochondrial evolution. *Cold Spring Harbor perspectives
903 in biology*, 4. Retrieved from <https://doi.org/10.1101/cshperspect.a011403> doi: 10.1101/cshperspect.a011403
- 904 Hahn, C., Bachmann, L., & Chevreux, B. (2013). Reconstructing mitochondrial
905 genomes directly from genomic next-generation sequencing reads—a baiting
906 and iterative mapping approach. *Nucleic Acids Research*, 41(13), e129. doi:
907 10.1093/nar/gkt371
- 908 Jin, J.-J., Yu, W.-B., Yang, J., Song, Y., dePamphilis, C. W., Yi, T.-S., & Li,
909 D.-Z. (2020). Getorganelle: a fast and versatile toolkit for accurate de
910 novo assembly of organelle genomes. *Genome Biology*, 21(1), 241. doi:
911 10.1186/s13059-020-02154-5
- 912 913 914

- 915 Judo, M. S. B., Wedel, W. R., & Wilson, B. H. (1998). Stimulation and sup-
916 pression of pcr-mediated recombination. *Nucleic Acids Research*, 26(7),
917 1819–1825. doi: 10.1093/nar/26.7.1819
- 918 Labrador, K., Agmata, A., Palermo, J. D., Ravago-Gotanco, R., & Pante, M. J.
919 (2021). Mitochondrial dna reveals genetically structured haplogroups of
920 bali sardinella (sardinella lemuru) in philippine waters. *Regional Studies in*
921 *Marine Science*, 41, 101588. doi: 10.1016/j.rsma.2020.101588
- 922 Li, H. (2018, 05). Minimap2: pairwise alignment for nucleotide sequences. *Bioin-*
923 *formatics*, 34(18), 3094-3100. Retrieved from <https://doi.org/10.1093/bioinformatics/bty191> doi: 10.1093/bioinformatics/bty191
- 925 Liang, Q., Bible, P. W., Liu, Y., Zou, B., & Wei, L. (2020, 02). Deepmi-
926 crobes: taxonomic classification for metagenomics with deep learning. *NAR*
927 *Genomics and Bioinformatics*, 2(1), lqaa009. Retrieved from <https://doi.org/10.1093/nargab/lqaa009> doi: 10.1093/nargab/lqaa009
- 929 Metzker, M. L. (2010). Sequencing technologies — the next generation. *Nature*
930 *Reviews Genetics*, 11(1), 31–46. doi: 10.1038/nrg2626
- 931 Mysara, M., Saeys, Y., Leys, N., Raes, J., & Monsieurs, P. (2015). Catch,
932 an ensemble classifier for chimera detection in 16s rrna sequencing stud-
933 ies. *Applied and Environmental Microbiology*, 81(5), 1573-1584. Retrieved
934 from <https://journals.asm.org/doi/abs/10.1128/aem.02896-14> doi:
935 10.1128/AEM.02896-14
- 936 Peccoud, J., Lequime, S., Moltini-Conclois, I., Giraud, I., Lambrechts, L., &
937 Gilbert, C. (2018, 04). A survey of virus recombination uncovers canon-
938 ical features of artificial chimeras generated during deep sequencing li-
939 brary preparation. *G3 Genes—Genomes—Genetics*, 8(4), 1129-1138. Re-
940 trieved from <https://doi.org/10.1534/g3.117.300468> doi: 10.1534/

- 941 g3.117.300468
- 942 Qin, Y., Wu, L., Zhang, Q., Wen, C., Nostrand, J. D. V., Ning, D., ... Zhou, J.
943 (2023). Effects of error, chimera, bias, and gc content on the accuracy of
944 amplicon sequencing. *mSystems*, 8(6), e01025-23. Retrieved from <https://journals.asm.org/doi/abs/10.1128/msystems.01025-23> doi: 10.1128/
945 msystems.01025-23
- 946
- 947 Qiu, X., Wu, L., Huang, H., McDonel, P. E., Palumbo, A. V., Tiedje, J. M., &
948 Zhou, J. (2001). Evaluation of pcr-generated chimeras, mutations, and het-
949 eroduplexes with 16s rrna gene-based cloning. *Applied and Environmental*
950 *Microbiology*, 67(2), 880–887. doi: 10.1128/AEM.67.2.880-887.2001
- 951 Ren, J., Song, K., Deng, C., Ahlgren, N., Fuhrman, J., Li, Y., ... Sun, F. (2020,
952 01). Identifying viruses from metagenomic data using deep learning. *Quan-*
953 *titative Biology*, 8. doi: 10.1007/s40484-019-0187-4
- 954 Rodriguez-Martin, B., Palumbo, E., Marco-Sola, S., Griebel, T., Ribeca, P.,
955 Alonso, G., ... Djebali, S. (2017, 01). Chimpipe: Accurate detection of
956 fusion genes and transcription-induced chimeras from rna-seq data. *BMC*
957 *Genomics*, 18. doi: 10.1186/s12864-016-3404-9
- 958 Rognes, T., Flouri, T., Nichols, B., Quince, C., & Mahé, F. (2016). Vsearch: a
959 versatile open source tool for metagenomics. *PeerJ*, 4, e2584. doi: 10.7717/
960 peerj.2584
- 961 Sedlazeck, F., Rescheneder, P., Smolka, M., Fang, H., Nattestad, M., von Haeseler,
962 A., & Schatz, M. (2018, 06). Accurate detection of complex structural
963 variations using single-molecule sequencing. *Nature Methods*, 15. doi: 10
964 .1038/s41592-018-0001-7
- 965 Sfeir, A., & Symington, L. S. (2015). Microhomology-mediated end joining: A
966 back-up survival mechanism or dedicated pathway? *Trends in Biochemical*

- 967 *Sciences*, 40(11), 701-714. Retrieved from <https://www.sciencedirect.com/science/article/pii/S0968000415001589> doi: <https://doi.org/10.1016/j.tibs.2015.08.006>
- 968
- 969
- 970 Vervier, K., Mahé, P., Tournoud, M., Veyrieras, J.-B., & Vert, J.-P. (2015, 11). Large-scale machine learning for metagenomics sequence classification. *Bioinformatics*, 32(7), 1023-1032. Retrieved from <https://doi.org/10.1093/bioinformatics/btv683> doi: 10.1093/bioinformatics/btv683
- 971
- 972
- 973
- 974 Willette, D., Bognot, E., Mutia, M. T., & Santos, M. (2011). *Biology and ecology of sardines in the philippines: A review* (Vol. 13; Tech. Rep. No. 1). NFRDI
- 975
- 976 Technical Paper Series. Retrieved from <https://nfrdi.da.gov.ph/tpjf/etc/Willette%20et%20al.%20Sardines%20Review.pdf>
- 977